THE JOURNAL OF PHYSICAL CHEMISTRY B

Article

pubs.acs.org/JPCB

Probing Methane Hydrate Nucleation through the Forward Flux Sampling Method

Yuanfei Bi and Tianshu Li*

Department of Civil and Environmental Engineering, George Washington University, Washington, D.C. 20052, United States

ABSTRACT: Understanding the nucleation of hydrate is the key to developing effective strategies for controlling methane hydrate formation. Here we present a computational study of methane hydrate nucleation, by combining the forward flux sampling (FFS) method and the coarse-grained water model mW. To facilitate the application of FFS in studying the formation of methane hydrate, we developed an effective order parameter λ on the basis of the topological analysis of the tetrahedral network. The order parameter capitalizes the signature of hydrate structure, i.e., polyhedral cages, and is capable of efficiently distinguishing hydrate from ice and liquid water while allowing the formation of different hydrate phases, i.e., sI, sII, and amorphous. Integration of the order parameter λ with FFS allows explicitly computing hydrate nucleation rates and obtaining an ensemble of nucleation trajectories under conditions where spontaneous hydrate nucleation becomes too slow to occur in direct simulation. The convergence of the obtained hydrate nucleation rate was found to depend crucially on the convergence of the spatial distribution for the spontaneously formed hydrate seeds obtained from the initial sampling of FFS. The validity of the approach is also verified by the agreement between the calculated nucleation rate and that inferred from the direct simulation. Analyzing the obtained large ensemble of hydrate nucleation trajectories, we show hydrate formation at 220 K and 500 bar is initiated by the nucleation events occurring in the vicinity of water−methane interface, and facilitated by a gradual transition from amorphous to crystalline structure. The latter provides the direct support to the proposed two-step nucleation mechanism of methane hydrate.

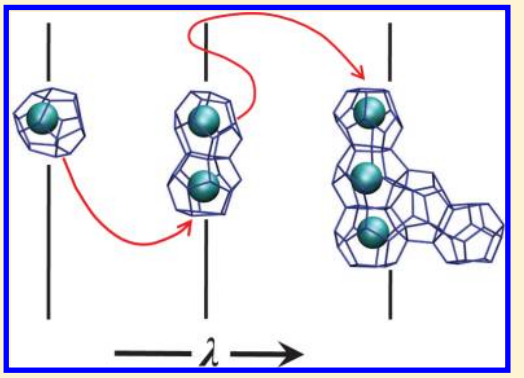

INTRODUCTION

Occurring both in nature and in man-made structures, methane hydrate plays a substantial role in energy recovery, flow assurance, global climate change, and gas storage/transportation.[1] The methane hydrates formed in ocean sediments and permafrost over million years store vast amount of energy, constituting a potential energy resource.[2] As a well-known hazard in petroleum industry, methane hydrate forms and accumulates unfavorably inside the oil and gas pipelines, clogging transmission lines and causing foremost safety issue. As a container for natural gas, gas hydrate holds an energy density comparable to that of compressed natural gas, which makes it promising to store and transport energy in solid hydrate form.[3,4] The significance of methane hydrates has attracted increasing attention of the ice-like crystals.

A thrust of current research of methane hydrate is the quantitative description of hydrate formation[5] so that the potential occurrence of hydrates can be predicted, and the strategies for controlling hydrates formation can be designed. To achieve this goal, a key step is to acquire the knowledge about hydrate formation at the molecular level. Different hypotheses[6−11] have been proposed to account for the nucleation of hydrate, but the verifications directly through experiments remain challenging due to the limited experimental resolution in probing such small and fast events. Molecular simulation, a computational tool for providing details at the molecular level, has been employed to unveil the nucleation mechanisms of methane hydrate.[7,9,10,12−17] Although significant progress has been made through the direct approach, much remains to be understood for the nucleation mechanisms and pathways under realistic thermodynamics conditions. In particular, sufficient statistical sampling is required to verify the proposed nucleation mechanisms.[18] Therefore, it is necessary to invoke advanced molecular simulation methods beyond the direct approach to gain the quantitative understanding of hydrate nucleation.

The main challenges in molecular simulations are primarily attributed to two types of slow dynamics present in the nucleation of solids in aqueous environment. The first type of slow dynamics is due to the sluggish motion of hydrogen-bonded tetrahedral network in supercooled water. The flexibility of hydrogen-bond yields a rough potential energy landscape, and the evolution of the tetrahedral network topology involves reorientation of hydrogen atoms, slowing down the dynamics. The second type of slow dynamics is associated with the rare event nature of nucleation process: Nucleation is a fluctuation-driven process, thus a long induction period is expected before the event of interest occurs. A large

Special Issue: Physics and Chemistry of Ice 2014

Received: March 26, 2014
Revised: May 21, 2014

   dx.doi.org/10.1021/jp503000u | J. Phys. Chem. B XXXX, XXX, XXX−XXX

free energy barrier prevents observing spontaneous nucleation in a small simulation cell.

In this study, we developed a computational strategy for studying hydrate nucleation by combining the forward flux sampling (FFS) method[19,20] and the recently developed coarse-grained mW water model.[21,22] The FFS method exploits the natural dynamics of the systems by dividing the full trajectory into consecutive segments, making it particularly suitable for modeling rare events of diffusive dynamics. The applicability of FFS in modeling nucleation under more realistic conditions, i.e., moderate or low supercooling, has been demonstrated by previous studies in silicon, germanium,[23,24] and water.[25,26] On the other hand, the mW water model[21] treats the water molecule as a single particle, with the tetrahedral strength between those of carbon and silicon. Omitting an explicit hydrogen bond, being short ranged, and free of electrostatic interaction, the mW water model offers much improved computational efficiency. Remarkably, the mW water model is capable of describing satisfactorily a wide range of thermodynamic properties of water and ice.[21]

When the FFS method is applied, an order parameter is needed to drive and characterize the progress of nucleation process. For monocomponent systems like water or silicon, the order parameter can be conveniently defined as the number of atoms or molecules contained in the largest crystalline cluster, on the basis of the effective means for distinguishing the solid-like particle from the liquid-like particle.[24,25] As methane hydrate is a nonstoichiometric, multicomponent system, and more importantly, the nucleation process can involve multi-steps, the choice of the order parameter is not as straightforward.[27−30] In this work, we have developed an effective order parameter on the basis of the topological analysis of the tetrahedral network and successfully integrated it with FFS. The method allows computing explicitly hydrate nucleation rate and obtaining ensemble of hydrate nucleation trajectories, at conditions where spontaneous nucleation is too slow to occur in the direct simulation.

The paper is organized as follows: First we describe the details of the computational method, in particular, the order parameter λ we have developed for the integration with the FFS method. In the following section, we report our investigations on the hydrate nucleation rate and show that the convergence of the computed nucleation rate depends on the initial sampling of FFS. The observed dependence will be discussed in conjunction with the analysis of the hydrate nucleation mode. Finally, the structure of hydrate nucleus will be analyzed, and a brief summary of the main results will conclude the paper.

METHODS

Forward Flux Sampling Method. In FFS, the rate constant is given by the "effective positive flux" expression:[31] $R = \dot{\Phi}_{\lambda_0} P(\lambda_n|\lambda_0)$, where $\dot{\Phi}_{\lambda_0}$ is the flux rate crossing the first interface, defined by the order parameter λ_0, and $P(\lambda_n|\lambda_0)$ is the probability for a trajectory starting from the interface λ_0 and successfully reaching the last interface λ_n. $\dot{\Phi}_{\lambda_0}$ can be computed by the direct molecular dynamics simulation through the relation $\dot{\Phi}_{\lambda_0} = N_0/(t_0 V)$, where N_0 is the number of direct crossing events of the first interface λ_0, t_0 is the total length of the direct simulation, and V is the volume of the water slab in the simulation cell. It should be noted that, although the calculation of flux rate $\dot{\Phi}_{\lambda_0}$ is straightforward, a sufficiently long direct simulation is needed in this step for obtaining the reliable rate, particularly in a nonhomogeneous system. The more challenging quantity to compute is $P(\lambda_n|\lambda_0)$. With the aid of the sampled interfaces λ_i between λ_0 and λ_n, one obtains $P(\lambda_n|\lambda_0) = \Pi_{i=1}^{n} P(\lambda_i|\lambda_{i-1}) = \Pi_{i=1}^{n} N_i/M_{i-1}$, where N_i is the number of successful crossing to the interface λ_i, and M_{i-1} is the number of the trial runs fired from the interface λ_{i-1}. Both N_i and M_{i-1} are obtained through FFS shooting procedures. The more details are explained in ref.[24,25]

Order Parameter λ. The order parameter λ is used to define the interfaces in FFS, and it plays two specific roles. (1) To drive the reaction along a predefined direction. In the case of hydrate nucleation, this direction refers to the formation of hydrate phases from a mixture of liquid water and methane gas. Therefore, the order parameter λ must be able to distinguish the products, e.g., hydrate phases, from the reactants, e.g., water−gas mixture. (2) To monitor the progress of the reaction. It is stressed that the order parameter λ is different from the actual *reaction coordinates* that specify the exact transition pathways. Instead, the order parameter λ only defines the stages of the reaction and allows the transition to follow freely the possible pathways. Similarly, λ should also be distinguished from the *local order parameter* that is used in the postprocessing to differentiate various products of a reaction. In contrast, the order parameter λ should be as inclusive as possible so that various structures are allowed to form and compete against each other during the formation process. It is crucial to develop an inclusive, not a specific, order parameter for identifying and validating the most relevant nucleation mechanism when there exist multiple nucleation pathways. This becomes particularly important for the study of hydrate nucleation where different hydrate phases, i.e., sI, sII, and amorphous, may all occur during the early stage of crystallization.

We note that the most prominent structural signature of methane hydrate is the polyhedral cages of water molecules. Water cages consist of nonplanar faces defined by hydrogen bonds of water molecules. In crystalline methane hydrate under low pressure, the most common water polyhedral cages are (1) a 5^{12} cage containing 12 five-membered rings (5MRs), (2) a $5^{12}6^2$ cage containing 12 5MRs and two six-membered rings (6MRs), and (3) a $5^{12}6^4$ cage containing 12 5MRs and four 6MRs. The methane hydrate crystalline structures are defined by the periodic combinations of these cages. The unit cell of structure I (sI) is composed of two 5^{12} cages and six $5^{12}6^2$, whereas the unit cell of structure II (sII) contains 16 5^{12} cages and eight $5^{12}6^4$ cages. The fourth type of water cage $5^{12}6^3$, which is not native to the crystalline phases, is commonly seen in the amorphous hydrate and interfaces between sI and sII hydrates. These cages do not occur in liquid water or crystalline ice, whereas the hydrate cluster grows through the agglomerate of the polyhedral cages. Therefore, an effective order parameter λ may reflect the formation and the attachment of polyhedral water cages. To identify the hydrate cluster from the liquid−gas mixture, we developed the following computational protocol.

1. A ring-statistics algorithm is employed to identify all the 5MRs and 6MRs in the liquid water. The 5MRs and 6MRs are the building blocks for the polyhedral cages in the methane hydrates.
2. A topological analysis is conducted to identify the formation of half-cages, i.e., 5^6, 5^66^1, and 5^66^2. The 5^6 half-cage is composed of 15 water molecules, making up

dx.doi.org/10.1021/jp503000u | J. Phys. Chem. B XXXX, XXX, XXX−XXX

one central 5MR and five peripheral 5MRs. The $5^6 6^1$ half-cage contains 18 water molecules and is arranged in a similar fashion as a 5^6 half-cage, except that the 6MR is at the center. The $5^6 6^2$ half-cage is assembled by two adjacent 5MRs surrounded by four 5MRs and two 6MRs, yielding a total of 20 molecules. The structures of these half-cages are shown in Figure 1.

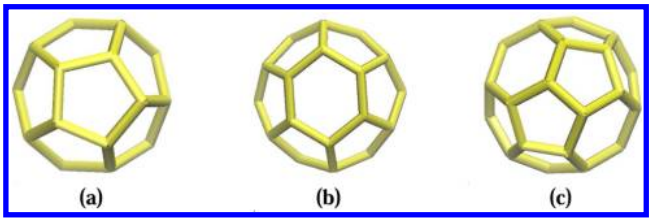

Figure 1. Three types of half-cages: (a) 5^6 half-cage, (b) $5^6 6^1$ half-cage, and (c) $5^6 6^2$ half-cage.

3. A cluster-walk algorithm is carried out to identify the connectivity of the half-cages. Two half-cages are defined to be connected if either of the following two criteria is met: (1) two half-cages share one and only one ring, regardless the types of the half-cages, and (2) two half-cages match their edges to form a complete cage. For (2), the following four types of complete cages can form via this definition: 5^{12}, $5^{12}6^2$, $5^{12}6^3$, and $5^{12}6^4$. It is noted that the $5^{12}6^3$ cage, which is not native to crystalline hydrate but does occur in amorphous hydrate and at the interface between sI and sII hydrates, is naturally included in the definition through joining a $5^6 6^1$ and a $5^6 6^2$ half-cage. Hydrate clusters in the liquid–gas mixture are obtained by iteratively finding all connected half-cages.

Protocols 1–3 allow identifying a hydrate-like cluster in a random tetrahedral network. The order parameter λ is subsequently defined as the size of the largest hydrate-like cluster for a configuration, namely, *the total number water molecules contained in the largest hydrate cluster*. The definition of order parameter λ has the following features.

First, the definition of the order parameter λ is conceptually simple but robust in differentiating hydrate from other phases. It capitalizes the formation of individual polyhedral cages, which are the fundamental building blocks of hydrates. Second, the defined order parameter λ imposes the formation of neither a particular hydrate phase nor a particular nucleation pathway. Because the ordering of polyhedral cages is not enforced by λ, the hydrate cluster is free to form sI, sII, or amorphous phase, and to evolve from one structure to another. It thus leaves it to the natural dynamics to determine how cages would be efficiently assembled to facilitate the phase transition. When the order parameter λ is combined with FFS method, it allows sampling an ensemble of nucleation pathways that vary both in the resulting hydrate structures and in their kinetics. Third, though our definition of order parameter is not focused on the ordering of guest molecules, we note that this information is included implicitly, as the formation of the water cages is typically facilitated by the ordering of guest molecules.[27] In addition, the parameter λ also permits the formation of empty cages, which may also occur during the crystallization of hydrates.[28,29,32]

It should also be mentioned that our current order parameter is focused on the three most commonly encountered half-cages, thus limiting the structure of hydrate to be composed of four major types of complete cages. However, the method can be conveniently extended to include more types of polyhedral cages that possibly exist in the noncrystalline hydrate and high-pressure crystalline phase sH. For example, the $4^1 5^{10} 6^2$ cage, a cage that involves the four-membered ring but may also find its appearance in the nucleation trajectories,[29,32,33] can be obtained by assembling 5^6 and $4^1 5^4 6^2$ half-cages. The identification of the latter half-cage would require searching for the four-membered rings in the tetrahedral network. In the cases where unknown types of polyhedral cages may contribute appreciably to the nucleation of hydrate, one may also redefine the order parameter on the basis of the FSICA method,[29] to include the general types of face-saturated incomplete cages.

Simulation Details. Our study employs a coarse-grained methane–water model where both water and methane are represented by single particles through the function form of Stillinger–Weber (SW) potential.[34] The mW water parameters are used for describing water–water interactions. The methane molecule, named as M in ref 9, interacts with other methane and water molecules through the two-body terms of SW potential. The simulation cell contains 6912 water molecules and 1280 guest molecules, with a periodic boundary condition (PBC) applied. The initial configuration of the methane–water mixture was prepared by melting an ice crystal containing 8192 water molecules and equilibrating liquid water at 300 K, followed by randomly converting 1280 water molecules into methane molecules. After further equilibration of the mixture at 300 K and 500 bar for 10 ns, a simulation cell containing aqueous and gas phases separated by the water–methane interfaces was obtained due to the low solubility of methane in water. The simulation cell was then slowly annealed to 220 K and equilibrated for over 200 ns at 220 K and 500 bar, to obtain the equilibrated water–methane interfaces. The final simulation cell is of an elongated tetragonal shape, with the dimensions of about $104 \times 52 \times 52$ Å^3. Due to the PBC, two water–methane interfaces are formed with a separation distance of about 72 Å enclosing an aqueous phase. The molar density profile of methane is shown in Figure 2. A time step of 10 fs is used in

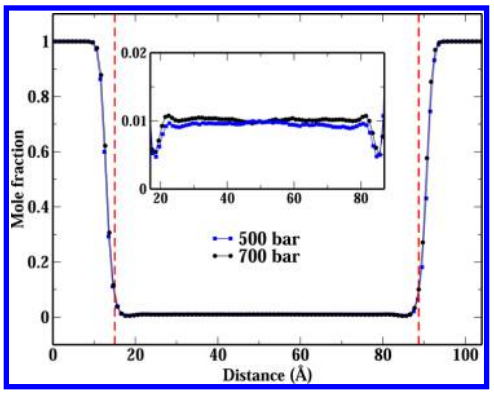

Figure 2. Molar density profile of methane normal to the water–methane interface at 220 K and 500 bar (blue square) and 220 K and 700 bar (black circle). The density profile was obtained using a bin size of 1 Å and averaging over the equilibrium MD trajectory of 300 ns. The dashed line defines the water–methane interface where the molar density of methane is 0.1. The inset shows the magnified density profile. The average solubility of methane in water is calculated to be 0.0096 ± 0.0003 and 0.0107 ± 0.0003 for 500 and 700 bar, respectively, at 220 K.

dx.doi.org/10.1021/jp503000u | J. Phys. Chem. B XXXX, XXX, XXX–XXX

our simulations. The isobaric−isothermal canonical ensemble (*NPT*) is employed with the relaxation time of 1 and 15 ps for controlling the temperature and pressure, respectively. A cutoff radius of 3.2 Å is used for identifying neighboring water−water molecules when the order parameter λ is computed. To further differentiate the hydrate structure in the formed hydrate nucleus, we employ the vertex order parameter ν_{jklm} developed by Jacobson et al.,[28] where the subscripts j ,k, l, and m denote the number of 5^{12}, $5^{12}6^2$, $5^{12}6^3$, and $5^{12}6^4$ cages surrounding a water vertex of the polyhedral cage, respectively. sI hydrate contains ν_{0400} and ν_{1300}, whereas sII hydrate yields ν_{4000}, ν_{3001}, and ν_{2002}. For effectively probing the local ordering in a small hydrate cluster, we slightly modified the definition of the vertex parameter such that the water molecules on the four neighboring cages of the vertex are considered to be of the same type as the vertex molecule. In addition, if a water molecule is classified as both sI- and sII-like, it will be redefined to be amorphous/interface-like.

For the computation of the nucleation rate, the FFS approach allows us to define the parameters, i.e., λ_i, N_i, and M_i, within a certain range without affecting the converged results. For example, in the current study, the following set of interfaces was used for the computation of $P(\lambda_n|\lambda_0)$ (Figure 4a and Figure 3b, t_0 = 483 ns): 19, 45, 60, 80, 100, 125, 150, 175, 200, 230, 260, 300, 350, and 400 for λ_A, λ_0, λ_1, ..., λ_{12}, respectively, where λ_A defines the boundary of basin A. As shown in Figure 3b, this set of parameters yields the same growth probability as that obtained by a different definition of interfaces used for t_0 = 312 ns, i.e., 19, 45, 60, 70, 80, 90, 100, 110, 120, 130, 140, 150, 160, 180, 200, 220, 250, and 280. For each interface, we collected N_i = 110−120 configurations from MD trial shootings, which corresponds to the number of trial shootings M_i ranging from 500 to 1500 for each interface with λ_i < 175, depending on the computed individual growth probability $P(\lambda_i|\lambda_{i-1})$. Such a large number of trial shootings ensures that the statistical uncertainty of the computed $P(\lambda_i|\lambda_{i-1})$ is less than 5% of $P(\lambda_i|\lambda_{i-1})$. For the interfaces with λ_i > 175, as the hydrate nucleus is approaching its critical size, $P(\lambda_i|\lambda_{i-1})$ becomes closer to unity, leading to a smaller number (120−500) of trial runs. The statistical uncertainty of the computed growth probability is mainly attributed to the error in the variance of the binomial distribution of N_i and the landscape variance of each configuration in the previous interface.[20] The critical size of hydrate nucleus can be computationally determined on the basis of the committor probability p_B.[35] As p_B measures the probability for a nucleus to grow into solid eventually, p_B = 0.5 implies that the complete dissolution and the complete growth of a cluster are equally likely, thus providing a good estimate of the critical size of hydrate nucleus. A typical simulation length for conducting the full FFS study is about 2.3 μs, with ∼0.5 μs for computing the initial flux rate, and ∼1.7 μs for computing the growth probability. The full convergence study (Results and Discussion and Figure 3b) amounts to a total simulation time of 8.3 μs.

RESULTS AND DISCUSSION

Nucleation Rate. We first focus on obtaining hydrate nucleation rate using the FFS method combined with our developed order parameter λ at 220 K and 500 bar. The nucleation temperature is 10 K higher than the condition (210 K and 500 bar) used in a previous study[9] that reported spontaneous hydrate nucleation in the direct molecular dynamics simulations. As the nucleation rate decreases sharply with the temperature, we expect that the spontaneous hydrate nucleation is unlikely to occur at 220 K. It is noted this temperature corresponds to about 71% supercooling with respect to the equilibrium melting temperature of sI structure at 500 bar.[36]

Different from homogeneous ice nucleation from supercooled water, hydrate nucleation occurs in a liquid−gas mixture that is a spatially heterogeneous system. A sufficient sampling of possible nucleation pathways is thus required to ensure the reliability of the computed nucleation rate. Therefore, it is necessary to perform a careful check on the convergence of the computed nucleation rate with respect to the parameters used in FFS. In particular, the computed growth probability $P(\lambda_n|\lambda_0)$ must converge with respect to the sampling of the flux rate $\dot{\Phi}_{\lambda_0}$. This is because the trial shootings for computing the growth probability is carried out using the initial configurations collected at interface λ_0, termed as "hydrate seeds" hereafter. As the system is inherently heterogeneous, a long simulation time is required to ensure the parameter space is sufficiently visited when $\dot{\Phi}_{\lambda_0}$ is computed.

Such need can be demonstrated in Figure 3b, which shows the computed growth probability $P(\lambda|\lambda_0)$ of hydrate nucleus as a function of nucleus size λ for different simulation length t_0 used in obtaining flux rate $\dot{\Phi}_{\lambda_0}$ (Figure 3a). It is evident that,

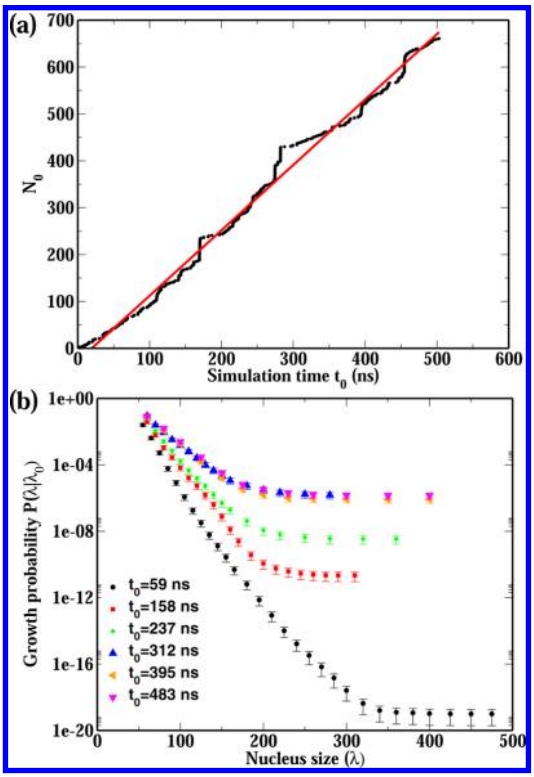

Figure 3. Computation of the nucleation rate at 220 K and 500 bar. (a) The number of initial configurations N_0 (shown as the black dots) collected at the first interface λ_0, as a function of simulation time t_0. By the slope of the curve ($(1.39 \pm 0.01) \times 10^9$ s^{-1}, obtained by linear regression, shown as the red line) and the volume of water slab (1.94×10^{-25} m^{-3})), one obtains the flux rate $\dot{\Phi}_{\lambda_0} = (7.18 \pm 0.04) \times 10^{33}$ m^{-3} s^{-1}. (b) The calculated growth probability $P(\lambda|\lambda_0)$ of the hydrate nucleus as a function of hydrate nucleus size λ for different simulation time t_0. The converged growth probability $P(\lambda|\lambda_0)$ is $(8.52 \pm 3.56) \times 10^{-7}$.

dx.doi.org/10.1021/jp503000u | J. Phys. Chem. B XXXX, XXX, XXX−XXX

though the computed growth probability achieves the relative convergence with respect to λ for a particular t_0, the absolute convergence of $P(\lambda|\lambda_0)$ is not obtained until the simulation length t_0 for sampling the initial configurations is greater than about 300 ns. As shown in the next section, the convergence of the computed growth probability is closely related to the convergence of the spatial distribution of the initial "hydrate seeds".

At 220 K and 500 bar, the calculated flux rate $\dot{\Phi}_{\lambda_0} = (7.18 \pm 0.04) \times 10^{33}$ m^{-3} s^{-1} and the growth probability $P(\lambda_n|\lambda_0) = (8.52 \pm 3.56) \times 10^{-7}$ yield a converged hydrate nucleation rate $R = (6.12 \pm 2.56) \times 10^{27}$ m^{-3} s^{-1}. The critical hydrate nucleus is estimated to contain around 240 water molecules, as shown in Figure 4b. On the basis of the computed nucleation rate, it is

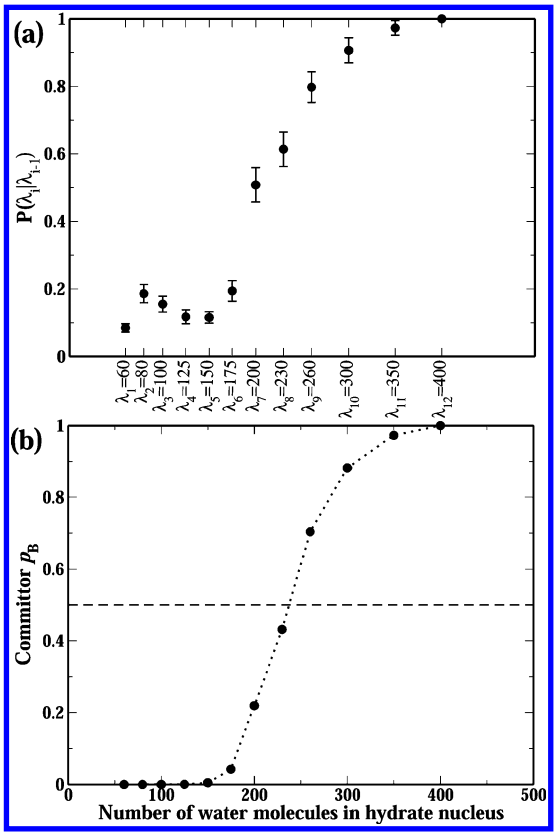

Figure 4. (a) Calculated individual growth probability $P(\lambda_i|\lambda_{i-1})$ for each interface λ_i at 220 K and 500 bar. (b) Calculated committor p_B as a function of the order parameter λ at 220 K and 500 bar. The critical size ($\lambda_c \approx 240$) is obtained by intersecting $p_B = 0.5$ (dashed line) with the computed p_B.

estimated that the observation of a spontaneous hydrate nucleation would require about 0.84 ms in a direct MD simulation using the same simulation cell.

To further confirm our approach is reliable in predicting hydrate nucleation rate, we carried out simulations at a higher pressure, i.e., 700 bar, where the increased pressure is expected to raise the hydrate nucleation rate so that spontaneous nucleation may occur in direct MD simulation. It is thus possible to compare directly the hydrate nucleation rate estimated from a direct MD simulation with that obtained from our approach. Indeed, a direct MD simulation at 220 K and 700 bar yields the spontaneous hydrate crystallization, as indicated by Figure 5, which shows the time evolution of the

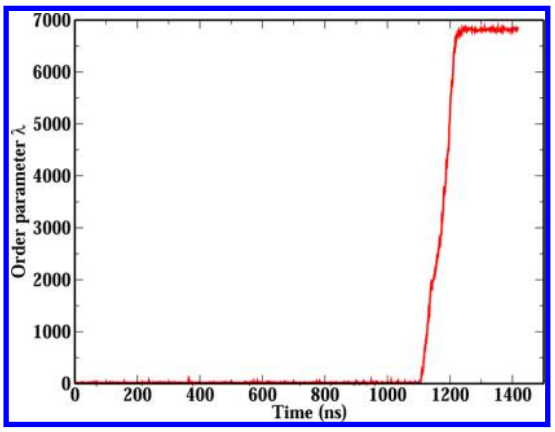

Figure 5. Time evolution of the order parameter λ, i.e., the total number of water molecules in the largest hydrate cluster, obtained from direct molecular dynamics simulation conducted at 220 K and 700 bar. The crystallization of hydrate starts at around 1100 ns and lasts for about ~110 ns until the entire aqueous phase turns into a hydrate.

order parameter λ. After about 1.1 μs of induction time, the hydrate nucleus starts forming, followed by a growth process that eventually turns supercooled aqueous solution into hydrate. The rate of hydrate nucleation, estimated on the basis of this single MD trajectory, is on the order of 10^{30} m^{-3} s^{-1}. For comparison, we carried out nucleation study at this condition using FFS approach and obtained the hydrate nucleation rate of $(7.11 \pm 2.40) \times 10^{29}$ m^{-3} s^{-1} (with $\dot{\Phi}_{\lambda_0} = (4.91 \pm 0.03) \times 10^{33}$ m^{-3} s^{-1} and $P(\lambda_n|\lambda_0) = (1.42 \pm 0.49) \times 10^{-4}$).

Nucleation Pathways. The large ensemble of hydrate nuclei stored at each interface allowed us to analyze the structural evolution and nucleation mechanism for each nucleation pathway. In particular, because the nucleation rate is controlled by the nucleation pathways that lead to the quickest hydrate formation, the explicitly computed nucleation rate would allow identifying the key nucleation mechanisms under the studied condition: The most pertinent nucleation mechanism must be the one that yields the highest hydrate nucleation rate. By analyzing nucleation trajectories, one can also gain insight on the key factors controlling the nucleation kinetics. Here we focus on two important aspects in the nucleation pathways, namely, the spatial distribution of hydrate nuclei and the evolution of hydrate structure.

Mode of Hydrate Nucleation. As liquid−gas mixture is spatially heterogeneous, it is of interest to understand where the hydrate nuclei are most likely to form. Figure 6a shows that the spatial distribution of the geometric center of the initial "hydrate seeds" is nonuniform along the direction normal to the water/methane interface. The nonuniformity can be attributed to the spatial heterogeneity of the liquid−gas mixture. In particular, it is evident that a higher distribution of hydrate nuclei is resulted in the vicinity of water/gas interface (i.e., peaks at $d_h = 5$ Å and $d_h = 12$ Å) than in the bulk aqueous solution.

Figure 6b shows the average distance $\bar{d}_h$ between the hydrate nucleus center and the water/methane interface, as a function of the size of the hydrate cluster λ at 220 K and 500 bar. The average $\bar{d}_h$ for small hydrate clusters ($\lambda = 45$) is located at about 18 Å from the interface, i.e., about one-half of the distance between the water/gas interface and the center of the bulk

dx.doi.org/10.1021/jp503000u | J. Phys. Chem. B XXXX, XXX, XXX−XXX

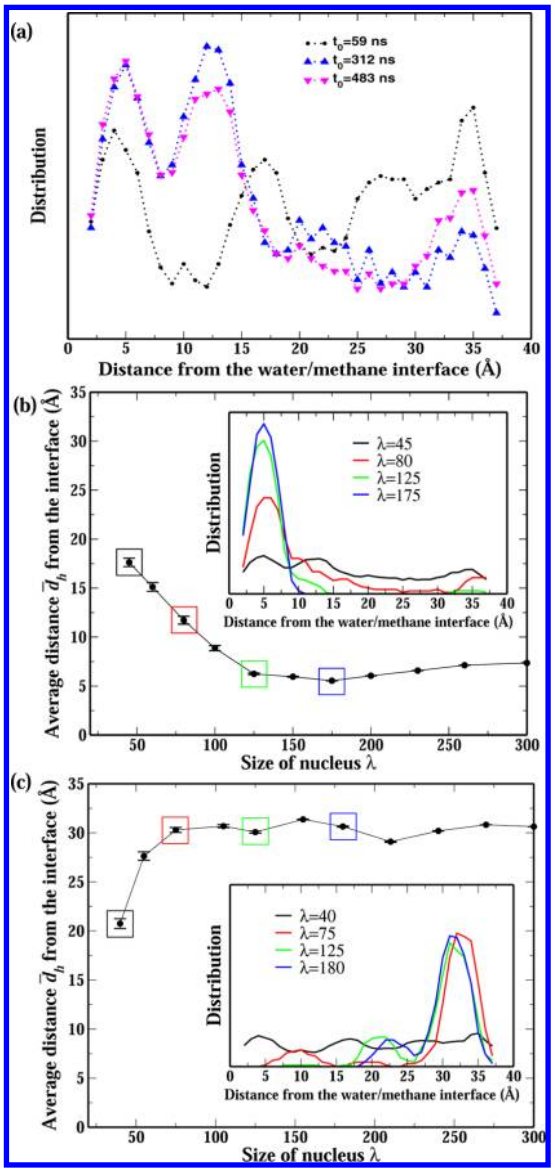

Figure 6. (a) Spatial distributions of the geometric centers of the "hydrate seeds" normal to the water−methane interface, obtained for different simulation time t_0. Note that the center of water slab is at about 36 Å from the interface. (b) Variation of the average distance $\bar{d}_h$ (from the hydrate nucleus geometric center to the water−methane interface) with the size of hydrate cluster λ, obtained on the basis of the initial sampling with t_0 = 485 ns. The inset shows the detailed spatial distributions of the geometric centers for the selected sizes marked, namely, λ = 45, 80, 125, and 175, respectively. (c) Same as (b), except that it is obtained on the basis of the initial sampling with t_0 = 59 ns.

liquid. This indicates that although hydrate seeds prefer to form near the interface, such a preference is not significant when the size of hydrate nucleus is small. As the hydrate nucleus grows, the average hydrate nucleus center appears to draw closer to the interface, attributed to the strong preference for hydrate nuclei to grow near the water/gas interface. Such a preference may be better illustrated by the inset of Figure 6b, which shows the detailed spatial distributions of the hydrate cluster center for different hydrate cluster sizes. As the hydrate nucleus grows, the distribution peak at d_h = 5 Å becomes more prominent, suggesting the hydrate nuclei in the vicinity of interface are more likely to grow. Because the FFS approach capitalizes the nucleation pathways yielding the highest nucleation rate among all the possible paths originated from the initial ensemble of "hydrate seeds" collected at λ_0, it is concluded that the calculated hydrate nucleation rate at 220 K and 500 bar is primarily determined by the hydrate nucleation occurring near the interface. This is not surprising as the density fluctuation of methane is more likely to reach the critical value[37] in the vicinity of interface where methane molecules are abundant. Recent neutron reflectivity study[38] also showed that hydrates form preferentially in the liquid−gas interface.

To unambiguously determine which mode, namely, surface mode or bulk mode, dominates hydrate nucleation under this condition, it may also be useful to estimate the nucleation rate for which the nucleation events were to only occur inside the bulk aqueous solution. Though such a rate may be calculated by using a "homogeneous" simulation cell[15] (i.e., no interface involved) containing a certain number of methane molecules corresponding to the equilibrium solubility under the same thermodynamic condition, we suggest that a reasonable estimate can already be made on the basis of our simulations using the "heterogeneous" liquid−gas mixture. As shown in Figure 6a, when a short simulation time, i.e., t_0 = 59 ns, was used to prepare the initial hydrate seeds, the spatial distribution of these hydrate nuclei is drastically different. The subsequent trial shootings based on these hydrate seeds yield the distinct pathways, as indicated by Figure 6c, which shows the nucleation of hydrate occurs in the bulk region of the water slab. Therefore, the nucleation of hydrate in this case is determined by the bulk mode. The corresponding growth probability (and nucleation rate) was found to be about 12 orders of magnitude smaller than that of the surface mode, as shown in Figure 3b.

It can be also seen that the convergence in the computed growth probability shown in Figure 3b is highly correlated to the convergence of the spatial distribution of the hydrate seeds. This explains why a long simulation time t_0 is needed to obtain a reliable nucleation rate in the heterogeneous system. It thus follows that the computed rate in such system may not be precise until the spatial distribution of the collected nuclei faithfully reflects that of a heterogeneous system. This observation can be used as a guideline for ensuring the reliability of the computed nucleation rate in a spatially heterogeneous system, on the basis of the FFS approach.

Structure of Hydrate Nucleus. Ostwald[39] pointed out over a century ago that the growing nuclei of solids do not necessarily have the structure of the thermodynamically stable phase but instead acquire a metastable structure. This rule, known as the Ostwald step rule, has been supported by many computer simulations of the nucleation of a variety of materials. For methane hydrate, recent studies[9,10,13,40] also reported that the initially formed water cages do not arrange themselves in an order consistent with those of crystalline phases. A two-step nucleation mechanism[8−10] was proposed to postulate that the formation of hydrate proceeds with the formation of amorphous hydrate nucleus, followed by a transformation into crystalline hydrate phase in the second stage. The two-step mechanism has seen supported by molecular simulations on its first part, i.e., the formation of amorphous hydrate nucleus. The second part of the mechanism, i.e., the transformation from amorphous to crystalline phase, has only been *indirectly* verified in molecular simulations[10,41] at temperatures higher than that of the actual nucleation event.

The obtained large ensemble of nucleation trajectories allow examining statistically the structure evolution of hydrate at the

dx.doi.org/10.1021/jp503000u | J. Phys. Chem. B XXXX, XXX, XXX−XXX

various stages of its crystallization. Figure 7 shows the average fractions of hydrate phases contained within a hydrate cluster,

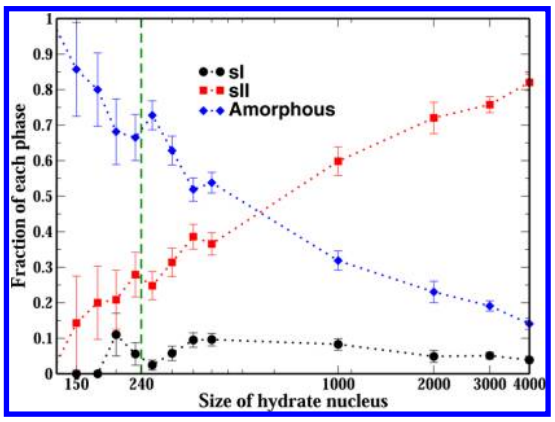

Figure 7. Variation of the average fraction of each phase of methane hydrate with the size of the hydrate nucleus λ. The green dash line indicates the critical nucleus size $\lambda_c = 240$ (see Figure 4b). The average fraction at each size is obtained on the basis of a total number of configurations about 110−120.

as a function of the size of the hydrate nucleus λ. Consistent with previous finding, hydrate clusters were found to adopt an amorphous structure initially. For example, Figure 7 shows that, on average, over 85% of the water molecules are amorphous-like in the hydrate nucleus containing 150 water molecules. As the hydrate nucleus grows, the fraction of the amorphous phase decreases steadily, yielding an increasing overall crystallinity. At the critical size ($\lambda_c \approx 240$), the amorphous hydrate phase accounts for about two-thirds of the hydrate nucleus, clearly indicating the nucleation of hydrate nucleus is controlled by the formation of noncrystalline phase under the simulation condition.

Our results further show that the crystallinity of hydrate cluster continues to develop in the growth stage. When the size of the hydrate λ reaches about 630, the fraction of the sII phase exceeds that of the amorphous phase, yielding a crystalline-dominated structure. The long-range crystalline ordering is illustrated in Figure 8, which shows the polyhedral cages nucleate at the water−methane interface and grow in parallel to it. The displayed long-ranged ordering corresponds to that of the sII hydrate, consistent with the analysis shown in Figure 7. Interestingly, Figure 7 also shows that there exists an anticorrelation between the fractions of amorphous phase and sII phase, implying that the vanishing amorphous phase is nearly entirely replaced by the sII phase. The sI phase, which has a higher equilibrium melting temperature than that of sII for the water−methane model used in this study, only accounts for less than 10% of the hydrate structure.

The occurrence of the sII phase in the spontaneously formed hydrate has been reported in both previous experimental[42,43] and simulation studies.[13,41] Although the exact origin is not clear, this result is not surprising in light of Ostwald's step rule. In the case of homogeneous ice nucleation, both experiments[44,45] and simulations[25,46] identify the structure of ice composed of disordered cubic and hexagonal stacking sequences. In the case of hydrate formation, experiments[47,48] and previous simulations[9] showed that in the early stage of crystal growth, the ratio of the fraction of small cage (5^{12}) to the fraction of large cages (combining all $5^{12}6^n$, $n = 2, 3, 4$), i.e., $f_{5^{12}}/f_{\text{large}}$, is significantly higher than that of sI phase (1/3), indicating the existence of the amorphous or sII phase. To make connection between the structure of the hydrate and the propensity of small and large cages, we analyze the average fraction of each type of polyhedral cage in the hydrate cluster along the crystallization trajectory. As shown in Figure 9, the small 5^{12} cage is prevalent overall. In contrast, although the large $5^{12}6^4$ cage is rare at the initial stage, its fraction increases

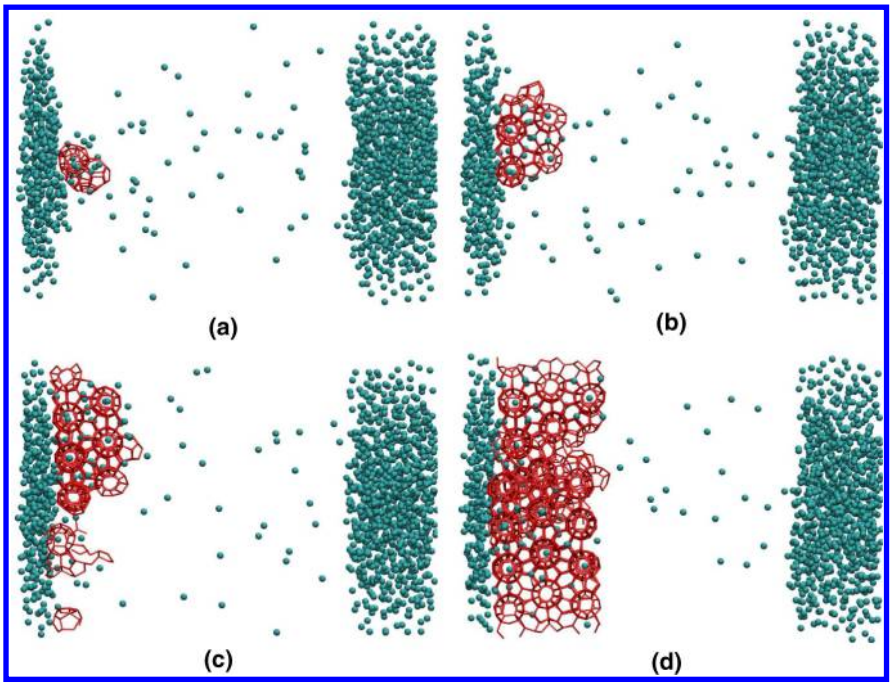

Figure 8. Trajectory of hydrate nucleation and growth at 220 K and 500 bar. (a)−(d) are the snapshots of the complete cages (red color) within hydrate nucleus containing 230, 400, 1000, and 2000 water molecules, respectively. The methane molecules are shown in green. The background water molecules are not shown.

dx.doi.org/10.1021/jp503000u | J. Phys. Chem. B XXXX, XXX, XXX−XXX

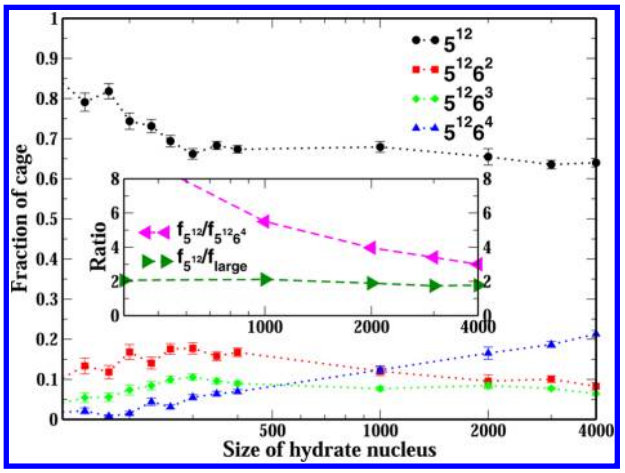

Figure 9. Variation of the average fraction for each type of cage with the size of hydrate nucleus λ. The inset shows the cage ratio between the small 5^{12} and the large $5^{12}6^4$ (magenta triangle), and between the small 5^{12} and all large cages combined (green triangle).

with the size of hydrate cluster. As a result, the ratio of small cage 5^{12} to the large cage $5^{12}6^4$ decreases quickly with the size. As shown in the inset of Figure 9, when a hydrate cluster contains 4000 water molecules, the ratio reaches about 3, already quite close to that of the sII phase. The converging of the ratio to sII is consistent with the increasing propensity of the sII phase in the crystallized hydrate phase.

CONCLUSIONS

We have investigated methane hydrate nucleation through applying the forward flux sampling method and the coarse-grained mW water model. To facilitate the application of FFS method in the nonstoichiometric binary system, we have developed an effective order parameter λ. The order parameter is constructed on the basis of the topological analysis of the tetrahedral network and capitalizes the signature of the hydrate phase--polyhedral cages. The order parameter not only can effectively distinguish the local hydrate phase from water and ice but, more importantly, allows the formation of various hydrate phases through different nucleation pathways.

By integrating the developed order parameter into the FFS method, we have explicitly computed the hydrate nucleation rate for the first time under conditions where spontaneous hydrate nucleation is unlikely to occur in direct simulations. At 220 K and 500 bar, the calculated hydrate nucleation rate is $R = (6.12 \pm 2.56) \times 10^{27}$ m^{-3} s^{-1}. Because hydrate nucleation occurs in the spatially heterogeneous water−methane system, the convergence of the computed hydrate nucleation rate was carefully checked. In particular, the computed hydrate nucleation rate shows a strong dependence on the initial sampling for computing the flux rate. At 220 K and 500 bar, our study showed that a direct MD simulation for the initial sampling with a minimum length of 300 ns is required to ensure the convergence of the calculated hydrate nucleation rate. Subsequent analysis on the nucleation pathways showed that the convergence of the computed hydrate nucleation rate is highly correlated with the convergence of the spatial distribution of the "hydrate seeds". A further validation was obtained by the agreement between the calculated nucleation rate with that inferred from the direct MD simulation, under 220 K and 700 bar where the spontaneous hydrate nucleation occurs at about 1.1 μs.

The analysis of the ensemble of hydrate nucleation pathways allowed revealing two interesting findings. First, our simulations demonstrated that the hydrate formation at 220 K and 500 bar is controlled by the surface mode; i.e., the critical hydrate nucleus forms in the vicinity of water−methane interface. This conclusion is supported by both the spatial distribution of hydrate nuclei and the inferred hydrate nucleation rate in the bulk mode (about 12 orders of magnitude smaller than that of the surface mode). Second, our simulation showed that hydrate tends to be amorphous-like upon the formation of the initial hydrate cluster and gradually transforms into crystalline structure as it grows. The observed evolution of hydrate structure, particularly the high crystallinity of the yielded hydrate phase, provides the direct support to the proposed two-step nucleation mechanism.

Finally, we stress that the observed hydrate nucleation behavior may only stand for its own under the studied condition, i.e., 220 K and 500 bar. Cautions need to be taken when hypothesizing nucleation behaviors under other conditions. Because of the complex nature of hydrate nucleation, it is likely that the most relevant pathways (hence nucleation mechanisms) may vary upon the change of the thermodynamic conditions. For example, Jacobson et al.[9] conducted direct MD simulation of hydrate nucleation at 210 K and 500 bar based on the same force field but did not observe the preference for surface nucleation. In our simulations under other conditions, we also found the surface mode may not be always favored. With the developed computational tool, it is now possible to examine explicitly the variation of nucleation rates, nucleation pathways, and nucleation mechanisms under various thermodynamic conditions. The discussions on this topic will be reported in another paper.

AUTHOR INFORMATION

Corresponding Author

*T. Li: e-mail, tsli@gwu.edu.

Notes

The authors declare no competing financial interest.

ACKNOWLEDGMENTS

The authors gratefully thank D. Donadio for sharing the ring statistics code. The work is supported by American Chemical Society Petroleum Research Fund and NSF through award CBET-1264438. T.L. also thanks the Sloan Foundation through the Deep Carbon Observatory for supporting this work.

REFERENCES

(1) Jr, E. D. S. Fundamental Principles and Applications of Natural Gas Hydrates. *Nature* **2003**, *426*, 353−359.
(2) Rath, B. Methane Hydrates: An Abundance of Clean Energy? *MRS Bull.* **2008**, *33*, 323−325.
(3) Rogers, R.; Zhong, Y. Feasibility of Storing Natural Gas in Hydrates Commercially. *Ann. N. Y. Acad. Sci.* **2000**, *912*, 843−850.
(4) Lee, H.; Lee, J.; Kim, D.; Park, J.; Seo, Y.; Zeng, H.; Moudrakovski, I.; Ratcliffe, C.; Ripmeester, J. Tuning Clathrate Hydrates for Hydrogen Storage. *Nature* **2005**, *434*, 743−746.
(5) Jr, C. R.; Lage, P. L. Modelling of Hydrate Formation Kinetics: State-of-the-art and Future Directions. *Chem. Eng. Sci.* **2008**, *63*, 2007−2034.
(6) Christiansen, R. L.; Sloan, E. D. Mechanisms and Kinetics of Hydrate Formation. *Ann. N. Y. Acad. Sci.* **1994**, *715*, 283−305.

(7) Radhakrishnan, R.; Trout, B. A New Approach for Studying Nucleation Phenomena Using Molecular Simulations: Application to CO2 Hydrate Clathrates. *J. Chem. Phys.* **2002**, *117*, 1786−1796.
(8) Guo, G.-J.; Li, M.; Zhang, Y.-G.; Wu, C.-H. Why Can Water Cages Adsorb Aqueous Methane? A Potential of Mean Force Calculation on Hydrate Nucleation Mechanisms. *Phys. Chem. Chem. Phys.* **2009**, *11*, 10427−10437.
(9) Jacobson, L. C.; Hujo, W.; Molinero, V. Amorphous Precursors in the Nucleation of Clathrate Hydrates. *J. Am. Chem. Soc.* **2010**, *132*, 11806−11811.
(10) Vatamanu, J.; Kusalik, P. G. Observation of Two-step Nucleation in Methane Hydrates. *Phys. Chem. Chem. Phys.* **2010**, *12*, 15065−15072.
(11) Walsh, M. R. Methane Hydrate Nucleation Rates and Mechanisms from Molecular Dynamics Simulations. *Ph.D. thesis*, Colorado School of Mines, 2011.
(12) Moon, C.; Taylor, P.; Rodger, P. Molecular Dynamics Study of Gas Hydrate Formation. *J. Am. Chem. Soc.* **2003**, *125*, 4706−4707.
(13) Walsh, M. R.; Koh, C. A.; Sloan, E. D.; Sum, A. K.; Wu, D. T. Microsecond Simulations of Spontaneous Methane Hydrate Nucleation and Growth. *Science* **2009**, *326*, 1095−1098.
(14) Walsh, M. R.; Beckham, G. T.; Koh, C. A.; Sloan, E. D.; Wu, D. T.; Sum, A. K. Methane Hydrate Nucleation Rates from Molecular Dynamics Simulations: Effects of Aqueous Methane Concentration, Interfacial Curvature, and System Size. *J. Phys. Chem. C* **2011**, *115*, 21241−21248.
(15) Sarupria, S.; Debenedetti, P. G. Homogeneous Nucleation of Methane Hydrate in Microsecond Molecular Dynamics Simulations. *J. Phys. Chem. Lett.* **2012**, *3*, 2942−2947.
(16) Knott, B. C.; Molinero, V.; Doherty, M. F.; Peters, B. Homogeneous Nucleation of Methane Hydrates: Unrealistic Under Realistic Conditions. *J. Am. Chem. Soc.* **2012**, *134*, 19544−19547.
(17) Liang, S.; Kusalik, P. G. Nucleation of Gas Hydrates within Constant Energy Systems. *J. Phys. Chem. B* **2013**, *117*, 1403−1410.
(18) Debenedetti, P. G.; Sarupria, S. Hydrate Molecular Ballet. *Science* **2009**, *326*, 1070−1071.
(19) Allen, R. J.; Frenkel, D.; Wolde, P. R. T. Simulating Rare Events in Equilibrium or Nonequilibrium Stochastic Systems. *J. Chem. Phys.* **2006**, *124* (024102), 1−16.
(20) Allen, R. J.; Frenkel, D.; Wolde, P. R. T. Forward Flux Sampling-type Schemes for Simulating Rare Events: Efficiency Analysis. *J. Chem. Phys.* **2006**, *124* (194111), 1−17.
(21) Molinero, V.; Moore, E. B. Water Modeled As an Intermediate Element between Carbon and Silicon. *J. Phys. Chem. B* **2009**, *113*, 4008−4016.
(22) Jacobson, L. C.; Molinero, V. A Methane-Water Model for Coarse-Grained Simulations of Solutions and Clathrate Hydrates. *J. Phys. Chem. B* **2010**, *114*, 7302−7311.
(23) Li, T.; Donadio, D.; Ghiringhelli, L. M.; Galli, G. Surface-induced Crystallization in Supercooled Tetrahedral Liquids. *Nat. Mater.* **2009**, *8*, 726−730.
(24) Li, T.; Donadio, D.; Galli, G. Nucleation of Tetrahedral Solids: A Molecular Dynamics Study of Supercooled Liquid Silicon. *J. Chem. Phys.* **2009**, *131* (224519), 1−7.
(25) Li, T.; Donadio, D.; Russo, G.; Galli, G. Homogeneous Ice Nucleation from Supercooled Water. *Phys. Chem. Chem. Phys.* **2011**, *13*, 19807−19813.
(26) Li, T.; Donadio, D.; Galli, G. Ice Nucleation at the Nanoscale Probes No Man's Land of Water. *Nat. Commun.* **2013**, *4* (1887), 1−6.
(27) Matsumoto, M. Four-Body Cooperativity in Hydrophonic Association of Methane. *J. Phys. Chem. Lett.* **2010**, *1*, 1552−1556.
(28) Jacobson, L. C.; Matsumoto, M.; Molinero, V. Order Parameters for the Multistep Crystallization of Clathrate Hydrates. *J. Chem. Phys.* **2011**, *135* (074501), 1−7.
(29) Guo, G.-J.; Zhang, Y.-G.; Liu, C.-J.; Li, K.-H. Using the Face-saturated Incomplete Cage Analysis to Quantify the Cage Compositions and Cage Linking Structures of Amorphous Phase Hydrates. *Phys. Chem. Chem. Phys.* **2011**, *13*, 12048−12057.
(30) Chakraborty, S. N.; Grzelak, E. M.; Barnes, B. C.; Wu, D. T.; Sum, A. K. Voronoi Tessellation Analysis of Clathrate Hydrates. *J. Phys. Chem. C* **2012**, *116*, 20040−20046.
(31) van Erp, T.; Moroni, D.; Bolhuis, P. A Novel Path Sampling Method for the Calculation of Rate Constants. *J. Chem. Phys.* **2003**, *118*, 7762−7774.
(32) Walsh, M. R.; Rainey, J. D.; Lafond, P. G.; Park, D.-H.; Beckham, G. T.; Jones, M. D.; Lee, K.-H.; Koh, C. A.; Sloan, E. D.; Wu, D. T. The Cages, Dynamics, and Structuring of Incipient Methane Clathrate Hydrates. *Phys. Chem. Chem. Phys.* **2011**, *13*, 19951−19959.
(33) Guo, G.-J.; Zhang, Y.-G.; Li, M.; Wu, C.-H. Can the Dodecahedral Water Cluster Naturally Form in Methane Aqueous Solutions? A Molecular Dynamics Study on the Hydrate Nucleation Mechanisms. *J. Chem. Phys.* **2008**, *128* (194504), 1−8.
(34) Stillinger, F. H.; Weber, T. A. Computer Simulation of Local Order in Condensed Phases of Silicon. *Phys. Rev., B Condens. Matter* **1985**, *31*, 5262−5271.
(35) Bolhuis, P. G.; Chandler, D.; Dellago, C.; Geissler, P. L. Transition Path Sampling: Throwing Ropes over Rough Mountain Passes, in the Dark. *Annu. Rev. Phys. Chem.* **2002**, *53*, 291−318.
(36) Jacobson, L. C.; Hujo, W.; Molinero, V. Nucleation Pathways of Clathrate Hydrates: Effect of Guest Size and Solubility. *J. Phys. Chem. B* **2010**, *114*, 13796−13807.
(37) Guo, G.-J.; Rodger, P. M. Solubility of Aqueous Methane under Metastable Conditions: Implications for Gas Gydrate Nucleation. *J. Phys. Chem. B* **2013**, *117*, 6498−6504.
(38) Koga, T.; Wong, J.; Endoh, M. K.; Mahajan, D.; Gutt, C.; Satija, S. K. Hydrate Formation at the Methane/Water Interface on the Molecular Scale. *Langmuir* **2010**, *26*, 4627−4630.
(39) Ostwald, W. The Formation and Changes of Solids. *Z. Phys. Chem.* **1897**, *22*, 289−330.
(40) Hawtin, R. W.; Quigley, D.; Rodger, P. M. Gas Hydrate Nucleation and Cage Formation at a Water/methane Interface. *Phys. Chem. Chem. Phys.* **2008**, *10*, 4853−4864.
(41) Jacobson, L. C.; Molinero, V. Can Amorphous Nuclei Grow Crystalline Clathrates? The Size and Crystallinity of Critical Clathrate Nuclei. *J. Am. Chem. Soc.* **2011**, *133*, 6458−6463.
(42) Fleyfel, F.; Devlin, J. P. Carbon Dioxide Clathrate Hydrate Epitaxial Growth: Spectroscopic Evidence for Formation of the Simple Type-II Carbon Dioxide Hydrate. *J. Phys. Chem.* **1991**, *95*, 3811−3815.
(43) Schicks, J.; Ripmeester, J. The Coexistence of Two Different Methane Hydrate Phases under Moderate Pressure and Temperature Conditions: Kinetic versus Thermodynamic Products. *Angew. Chem. Int. Ed.* **2004**, *43*, 3310−3313.
(44) Malkin, T. L.; Murray, B. J.; Brukhno, A. V.; Anwar, J.; Salzmann, C. G. Structure of Ice Crystallized from Supercooled Water. *Proc. Natl. Acad. Sci. U. S. A.* **2012**, *109*, 1041−1045.
(45) Kuhs, W. F.; Sippel, C.; Falenty, A.; Hansen, T. C. Extent and Relevance of Stacking Disorder in "Ice Ic. *Proc. Natl. Acad. Sci. U. S. A.* **2012**, *109*, 21259−21264.
(46) Moore, E. B.; Molinero, V. Is It Cubic? Ice Crystallization from Deeply Supercooled Water. *Phys. Chem. Chem. Phys.* **2011**, *13*, 20008−20016.
(47) Moudrakovski, I. L.; Sanchez, A. A.; Ratcliffe, C. I.; Ripmeester, J. A. Nucleation and Growth of Hydrates on Ice Surfaces: New Insights from 129Xe NMR Experiments with Hyperpolarized Xenon. *J. Phys. Chem. B* **2001**, *105*, 12338−12347.
(48) Klapproth, A.; Goreshnik, E.; Staykova, D.; Klein, H.; Kuhs, W. F. Structural Studies of Gas Hydrates. *Can. J. Phys.* **2003**, *81*, 503−518.